NANO LETTERS

pubs.acs.org/NanoLett Letter

Observation of Invisibility Angle and Flat Band Physics in Dipolar Photonic Lattices

Diego Román-Cortés,[¶] Maxim Mazanov,[¶] Rodrigo A. Vicencio,[*] and Maxim A. Gorlach[*]

Cite This: *Nano Lett.* 2025, 25, 4291−4297 Read Online

ACCESS | Metrics & More | Article Recommendations | Supporting Information

ABSTRACT: Evanescently coupled waveguide arrays provide a tabletop platform to realize a variety of Hamiltonians, where physical waveguides correspond to the individual sites of a tight-binding lattice. Nontrivial spatial structure of the waveguide modes enriches this picture and uncovers further possibilities. Here, we demonstrate that the effective coupling between *p*-like modes of adjacent photonic waveguides changes its sign depending on their relative orientation vanishing for proper alignment at a so-called *invisibility angle*. Using femtosecond laser-written waveguides, we demonstrate this experimentally for *p*-mode dimers and graphene-like photonic lattices exhibiting quasi-flat bands at this angle. We observe diffraction-free propagation of corner and bulk states, providing robust experimental evidence of a two-dimensional Aharonov−Bohm-like caging in an optically switchable system.

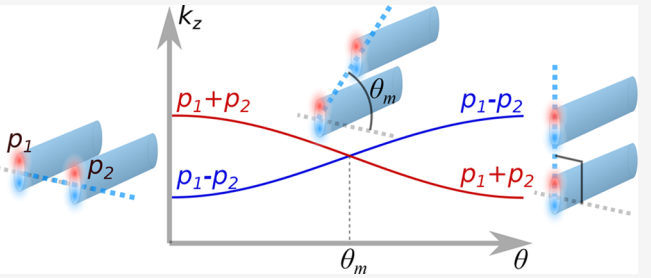

KEYWORDS: *flat bands, Aharonov−Bohm caging, photonic orbitals, laser-written waveguides*

Photonic lattices have emerged as a versatile platform to explore localization and transport phenomena.[1−3] As the paraxial equation governing light propagation in a single waveguide resembles Schrödinger equation in quantum mechanics, arrays of evanescently coupled waveguides provide a straightforward realization of paradigmatic tight-binding models[4] with the possibility to accommodate such exotic features as negative couplings,[5,6] artificial gauge fields,[2,7] and non-Hermitian physics.[8−10]

The development of this platform exhibits profound parallels with condensed matter physics and materials science[11] as illustrated in Figure 1. On a qualitative level, the formation of a material can be sketched as a coupling of atoms and formation of molecules; hybridization of molecular orbitals results in molecular aggregates and, finally, in the emergence of a 2D material. In the same spirit, the waveguides can be strongly coupled to each other to form photonic molecules.[12] The collective modes of those molecules with distinct symmetry can be readily identified as different orbitals, and their overlap determines the properties of a given photonic lattice. This parallel appears to be especially fruitful in light of the recent studies which demonstrated photonic molecule concept experimentally[12] and predicted a vast range of novel functionalities, including topological phases[13,14] mediated by the coupling between different photonic orbitals.[15−18]

Here, we add a crucial ingredient to this picture by introducing an *invisibility angle* in the photonic lattices. Specifically, we demonstrate theoretically and experimentally that a suitable arrangement of optical waveguides hosting *p*-type orbital modes results in a vanishing effective coupling between them. As a result, the lattice of such waveguides features dispersionless bulk modes unlocking an all-bands-flat regime (ABF).[19−21] A distinctive feature of this regime is photonic Aharonov−Bohm (AB) caging when an arbitrary initial state does not diffract into the bulk of the lattice, remaining confined in a finite spatial region, oscillating, and periodically recovering its initial profile.

The idea of an invisibility angle has some parallels with the magic angle concept in condensed matter literature,[22] where it was introduced to denote unconventional electronic properties of twisted bilayer graphene, with flat bands and resulting superconducting behavior.[23,24] The advancement of this concept resulted in the field of twistronics[25] spanning such disciplines as condensed matter physics, polaritonics, and photonics.[26,27]

The origin of the flat bands can be traced to the compact localized states,[28−31] which are perfectly confined lattice eigenmodes. Typically, flat bands in tight-binding lattices arise due to the destructive interference in the so-called connector sites[32−35] and require fine-tuning of the lattice parameters.[19,36] However, having an *all* band flat regime is much less trivial. While in optical one-dimensional systems the ABF regime could be achieved by several means including multiorbital mechanisms[6,15,16,37−39] or effective magnetic

Received: November 26, 2024
Revised: February 11, 2025
Accepted: March 3, 2025
Published: March 6, 2025

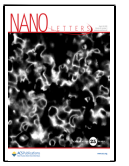

https://doi.org/10.1021/acs.nanolett.4c05951
Nano Lett. 2025, 25, 4291−4297

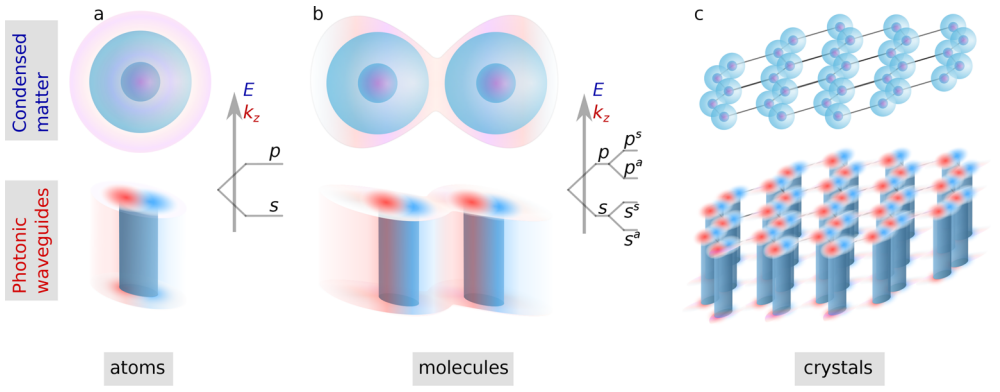

Figure 1. Parallels between condensed matter systems and photonic lattices: (a) individual atoms, (b) molecules, and (c) 2D crystals. Classical light propagation in waveguide arrays models the temporal evolution of condensed matter systems. Second row illustrates *p*-mode waveguides (a) as promising artificial-atom building blocks which could be utilized in photonic molecules with nontrivial phase profiles (b) and flat-band photonic lattices (c). Zero coupling between the *p* modes at invisibility angle decomposes the modes of a *p*-mode graphene-like lattice into isolated compact localized states rendering all bands flat.

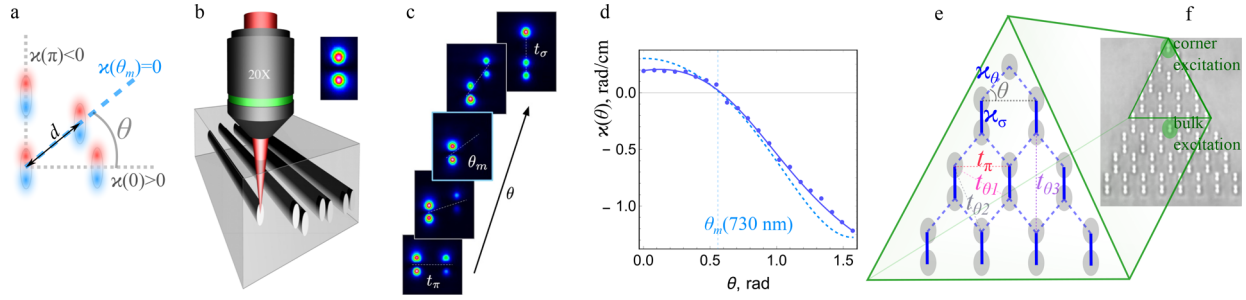

Figure 2. The invisibility angle concept and *p*-mode graphene-like lattice. (a) Coupling between the pair of identical *p*-mode optical waveguides vanishes at invisibility angle θ_m. (b) Illustration of the femtosecond laser writing technique for the waveguide dimers. The inset shows an experimental *p*-mode intensity profile after excitation via the spatial light modulator (SLM),[48] at the working wavelength 730 nm. (c) Dimer intensity profiles for the propagation distance of L = 25 mm after SLM excitation at the left waveguide. (d) Experimentally extracted *p*-mode coupling $\kappa(\theta)$ (blue dots, with a solid line as a guide to the eye) and numerically calculated coupling from collective dimer propagation constants (dashed line). (e) Sketch of the graphene-like lattice with fixed nearest-neighbor distance d, two dominant couplings χ_σ and χ_θ indicated by solid and dashed lines, respectively, as well as long-range couplings t_π and $t_{\theta 1}$−$t_{\theta 3}$. (f) White light microscope image of a fabricated lattice with bulk and corner excitation spots highlighted in green.

fields[6,7,21,40,41] allowing achievement of $Q \sim 3$−5 Aharonov−Bohm caging cycles for a point excitation, its realization in two dimensions remains challenging. Known theoretical proposals of Bloch ABF phases[40] are based on $\mathcal{T}_3$ (dice) and $\mathcal{T}_4$ lattices in external magnetic field and found experimental realizations in wire networks.[42] Although these two-dimensional models are generalizations of the one-dimensional rhombic lattice in external magnetic field, they cannot be straightforwardly implemented in generic optical setups such as optical waveguide lattices with symmetric (monopolar) modes as they require vanishing couplings in some directions. Thus, finding an alternative approach in the optical domain remains a challenge.

A separate line of research in photonic ABF phases aims to design Landau levels in nonperiodic lattices. However, the application of this strategy to the optical range remains challenging. In the telecom frequency range, photonic crystal platform with effective strain was recently proposed[43] to generate several quasi-flat Landau minibands in a silicon photonic crystal while leaving other bands dispersive. Recent experiment in ref 44 fixes this issue by the careful design of the couplings pattern. Nevertheless, that structure operates only in the microwave frequency range. Importantly, systems with Landau levels feature multiple groups of mini-flat-band (non-Bloch) modes with reduced density of states scaling as $\sim\sqrt{N}$, where N is the number of sites in the lattice, while the density of states for flat Bloch bands in periodic lattices scales as $\sim N$. The density of states is a key factor in such applications of all-bands-flat physics as enhancement of nonlinear phenomena, stronger light−matter interactions and lasing applications,[32−35] making periodic realizations especially favorable. Hence, an experimental realization of the ABF regime in optical periodic two-dimensional lattices remains an important open fundamental problem.

In this article, we experimentally realize for the first time a nearly all-bands-flat regime in an optical periodic lattice by harnessing the invisibility angle paradigm. We start from a pair of interacting *p*-mode waveguides identifying the conditions for a zero coupling between them at invisibility angle. Next, we arrange the waveguides into a graphene-like lattice and predict the formation of quasi-flat bands. Compared to the one-dimensional models, the effect of long-range couplings starts to play an increasingly important role, while there are significant complications in managing the directionality of the couplings in the optical range. Despite that, we demonstrate $Q \sim 3$ Aharonov−Bohm caging cycles for the generic point of initial excitation, thanks to the invisibility angle concept. By imaging the intensity distribution at the output, we demonstrate a

https://doi.org/10.1021/acs.nanolett.4c05951
Nano Lett. 2025, 25, 4291−4297

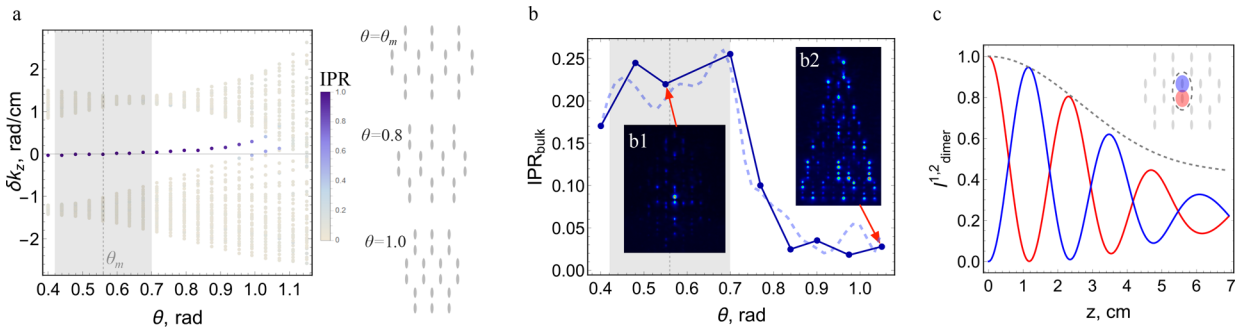

Figure 3. Bulk flat bands and photonic Aharonov–Bohm caging. (a) Spectrum of the propagation constants for a finite 15-row graphene-like lattice calculated for numerically retrieved couplings depending on angle θ for d = 25 μm and λ = 730 nm. Color encodes the localization of the modes. This includes the effect of long-range couplings and the nonorthogonality correction. Right insets show the geometry of the lattice for several representative θ. (b) Values of inverse participation ratio (IPR) versus angle θ for a bulk site SLM excitation. Dotted line shows simulated results, dots with solid approximating line depict experimental data. We observe a plateau behavior with nearly isolated dimer dynamics at angles around the invisibility angle $\theta_m \simeq 0.56$ (gray shaded area). Insets show experimental propagated intensity profiles for two angles highlighted by arrows. (c) Numerically propagated intensities for $\theta = \theta_m$ after bulk excitation (red, its dimer partner in blue) show an oscillating behavior indicative of photonic caging with almost three full caging cycles at the lattice output facet. Gray dashed line shows the total dimer intensity.

diffraction-suppressed propagation of bulk and topological corner modes of the designed lattice.

INVISIBILITY ANGLE FOR *P*-MODE WAVEGUIDES

In the case of two parallel electric dipoles, simple electrostatic calculation suggests that their interaction vanishes at an angle $\theta_0 = \arcsin(1/\sqrt{3}) \approx 0.615$ rad when the dipoles are perfectly decoupled. Though this idea has been appreciated in chemistry,[45,46] it breaks down at nonzero frequencies. In contrast, the invisibility angle in photonics (Figure 2a) persists in a wide frequency range. As the coupling between the two evanescent waveguide modes is determined by their overlap integral,[10,47] the signs of the coupling can be read off from Figure 2a. For horizontal positioning ($\theta = 0$), both pairs of the closest lobes are in phase resulting in positive coupling, while for vertical positioning ($\theta = \pi/2$) the overlap integral is negative dominated by the interaction of the two opposite-phase lobes. Since the coupling varies continuously, a special angle θ_m exists such that coupling $\kappa(\theta_m) = 0$.

To probe the interaction between the p modes experimentally, we fabricate pairs of elliptical waveguides with vertically oriented p modes utilizing a femtosecond laser writing technique,[1,48] Figure 2b. Launching light in one of the waveguides, we track intensity beatings in the dimer (Figure 2c) by retrieving the absolute value of the effective coupling constant. The coupling sign is chosen based on the continuity of $\kappa(\theta)$ function and assuming $\kappa(0) > 0$, $\kappa(\pi/2) < 0$.

In particular, experiments with p dimers at a distance d = 25 μm and wavelength λ = 730 nm yield an invisibility angle $\theta_m \approx$ 0.56 rad, not much different from the one predicted in electrostatics. Experimentally retrieved values of the coupling constant κ for various θ values are depicted in Figure 2d. Numerical calculations in COMSOL Multiphysics, with refractive index n = 1.48 (borosilicate), elliptical waveguide profiles with a fine-tuned contrast of $\delta n = 10^{-3}$, semiaxes a = 2.45 μm and b = 8.18 μm,[48] fully support these findings as shown by the dotted line in Figure 2d.

OPTICAL GRAPHENE-LIKE LATTICE

In turn, invisibility angle physics has a profound effect on the behavior of p-waveguide optical lattices. To illustrate that, we design and fabricate a set of 9 graphene-like structures consisting of identical p-mode waveguides with a fixed distance d between the nearest neighbors (Figure 2e,f). The properties of the lattices are then controlled by the angle θ defining the degree of geometric deformation and varying from sample to sample (Figure 2e). Qualitatively, if coupling κ_θ vanishes, the lattice decomposes into isolated dimers with two fully flat bulk bands formed by symmetric and antisymmetric dimer modes. The isolated upper corner site in a finite triangular sample forms a "zero-energy" corner-state in the middle of the bandgap.

Realistically, the photonic bands do not become fully flat. Although the nearest-neighbor coupling κ_θ is tuned to be zero at the invisibility angle, long-range couplings t_π and $t_{\theta 1}$–$t_{\theta 3}$ have to be taken into account as well. Nearest-neighbor and longer-range couplings comprise the Hermitian coupling matrix of the form

$$\hat{H}_\Sigma = \hat{H}_{NN} + \hat{H}_{NNN} + \hat{H}_{NNNN} \tag{1}$$

where $\hat{H}_{NN}$ includes two major nearest-neighbor couplings κ_θ and κ_σ, $\hat{H}_{NNN}$ includes two next-nearest-neighbor couplings t_π and $t_{\theta 2}$, and $\hat{H}_{NNNN}$ includes two longer-range couplings $t_{\theta 1}$ and $t_{\theta 3}$, as depicted in Figure 2e (see details in Supporting Information[48]).

Furthermore, the modes of isolated waveguides which are used as a basis for the tight-binding description, are not quite orthogonal, as there is a nonzero overlap between them quantified by the coefficients

$$c_{ij} = \frac{1}{I} \iint E_j(x, y)\, E_i^*(x, y)\, \mathrm{d}x\, \mathrm{d}y \tag{2}$$

where $I = \iint |E_i(x,y)|^2\, \mathrm{d}x\, \mathrm{d}y = \iint |E_j(x,y)|^2\, \mathrm{d}x\, \mathrm{d}y$ and $E_{i,j}$ are the electric field profiles at waveguides i and j, respectively. Note that nonorthogonality corrections become especially pronounced for small ($\theta < 0.4$ rad) and large ($\theta > 0.9$ rad) angles resulting in a modified propagation equation[4,49,50]

$$-i\frac{\mathrm{d}\psi(z)}{\mathrm{d}z} = \hat{c}^{-1}\hat{H}_\Sigma \psi(z) \tag{3}$$

where $\psi(z)$ is a vector constructed from the amplitudes of the waveguide fields. The matrix $\hat{H}'_\Sigma = \hat{c}^{-1}\hat{H}_\Sigma$ governs light propagation providing the Hamiltonian of the lattice.

https://doi.org/10.1021/acs.nanolett.4c05951
Nano Lett. 2025, 25, 4291–4297

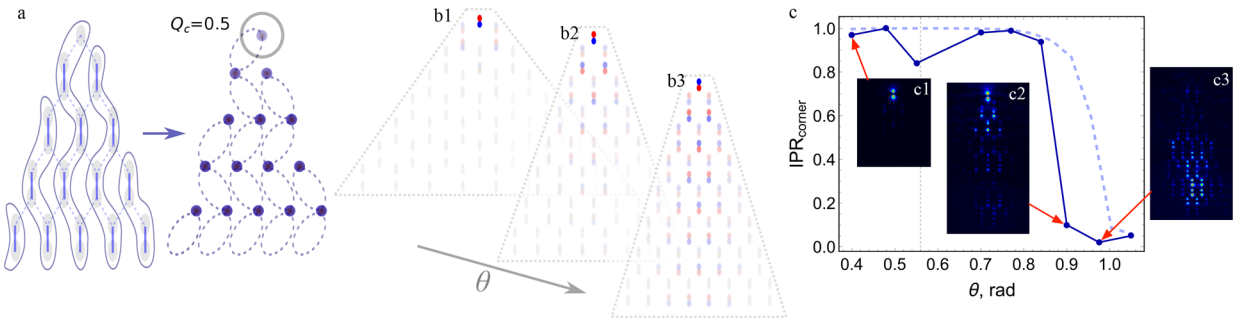

Figure 4. Topological corner state. (a) Wannier centers following from the flat-band limit decomposition of the lattice into SSH arrays of isolated dimers indicate the effective corner charge Q_c = 0.5 and quantized bulk polarization P = (0.5, 0.5). (b1−b3) Amplitude profiles of the topological corner state in three finite lattices for the wavelength λ = 730 nm and three angles θ_{1-3} = 0.4, 0.9, and 0.975 rad. (c) Inverse participation ratio for the output field demonstrates a localization transition at large angles θ > 0.9 rad. Insets depict the experimental intensity profiles for geometries b1−b3, respectively.

As the chosen basis of the individual waveguide modes is nonorthogonal, the Hamiltonian $\hat{H}'_\Sigma$ is non-Hermitian. However, such non-Hermiticity is an artifact which is readily removed by the suitable nonunitary linear transformation to a new orthogonalized basis.[50] In particular, in the basis defined by the nonunitary transformation matrix $\hat{T}$ such that $\hat{c} = \hat{T}^\dagger\hat{T}$, the Hermitian Hamiltonian reads $H''_\Sigma = (\hat{T}^\dagger)^{-1}\hat{H}_\Sigma\hat{T}^{-1}$ and has the same spectrum as $\hat{H}'_\Sigma$. As a consequence, the entire dynamics is Hermitian, and the spectrum of propagation constants is real. The latter can be recovered from both the Hermitian Hamiltonian in the transformed basis H''_Σ or the initial matrix $\hat{H}'_\Sigma$. In turn, the spectrum of the Hamiltonian $\hat{H}'_\Sigma$ fully agrees with the results of full-wave numerical simulations in COMSOL Multiphysics (see Supporting Information section III[48]).

The results computed for a finite lattice, taking into account both long-range couplings and nonorthogonality corrections, are presented in Figure 3a. We observe that the spectrum indeed contains nearly flat bands persisting in the entire region of angles θ highlighted in Figure 3a by gray.

Along with the nearly flat bands, we find a localized corner state near the center of the bandgap with high inverse participation ratio[51] IPR = $\sum_i I_i^4/(\sum_i I_i^2)^2 \approx 1$. Here, I_i is the intensity at ith site and the sum runs over all sites of the lattice. Notably, the corner mode arises in the middle of the bandgap in the same θ interval, shifting away from the bandgap center for larger angles.

BULK DYNAMICS AND AHARONOV−BOHM CAGING

We probe the flat-band dynamics experimentally by exciting a single bulk site (see Figure 2f) on a set of 9 graphene-like lattices fabricated on a L = 70 mm long glass wafer.[48] In this case, we use a spatial light modulator setup[48] and track the propagated intensity profiles at the output, as shown in Figure 3b. We then postprocess the data to extract the inverse participation ratio (IPR) quantifying the localization of the field: higher IPR indicates stronger field confinement. As the initial single-site excitation has nonzero projections on all Bloch bands, this experiment tests the dispersion of all bulk bands. Thus, near-diffractionless propagation implies significant flatness of all bands.[7,37,38]

The analyzed data show two distinct regimes: for lattices with 0.4 < θ < 0.8 close to the invisibility angle a good caging effect is observed. However, larger angles (θ > 0.8) favor a significant field diffraction; therefore, the field at the output is delocalized. These experimental results shown in Figure 3b by the dots are in very good agreement with the theoretical calculation (dashed line). Thus, contrary to the expectation that the long-range couplings and nonorthogonality corrections could degrade the flat-band dynamics,[49,52] in our lattice weak long-range couplings do not destroy the quasi-flat band physics around the invisibility angle. The maximum value for the inverse participation ratio (IPR) of 0.20−0.25 for the bulk dimer state after three AB caging cycles also suggests rather pronounced localization comparable with one-dimensional optical ABF proposals.[6,7,21,37]

Numerical simulations of the field propagation for the excited dimer near the invisibility angle show a coherent and slowly decaying oscillating behavior which is characteristic of caging effects in the presence of small band dispersion, with nearly three full cycles of caging dynamics shown in Figure 3c. This indicates similar or even increased caging fidelity compared to the recent 1D photonic proposals.[6,7,37] The excited region coincides with the dimer compact localized states (CLS), being therefore the smallest observed flat band state in 2D lattices,[35,53,54] similar to CLS observed in 1D systems.[55] This further confirms the quasi-flat band dynamics arising due to the invisibility angle effect. Interestingly, our structure has an almost perfectly flat upper band, see Supporting Information Figure S3c,d.[48] Thus, the initial excitations formed entirely from the states of this flat band could in principle give rise to an even larger number of Aharonov−Bohm caging cycles.

CORNER STATE EXCITATION

Another alternative is to excite the corner site of the fabricated graphene-like lattice (Figure 2e), which is expected to decouple from the rest of the structure in the idealized invisibility angle limit. In this case, the lattice decomposes into isolated dimers, which could be further grouped into vertical quasi-one-dimensional Su−Schrieffer−Heeger (SSH) arrays,[56] as described in Figure 4a. Note that only one of those chains has a nontrivial charge Q_c = 0.5 at the edge, quantized by the inversion symmetry.[57]

This atomic limit is adiabatically connected to all realistic configurations which still respect inversion symmetry, and thus the corner charge persists for the full Hamiltonian $\hat{H}''_\Sigma$. A direct calculation of Wannier centers[48] yields bulk polarization P = (0.5, 0.5), quantized by the inversion symmetry. Together with the corner charge, this allows us to classify the corner mode as a Wannier-type higher-order topological one in the $h_{1b}^{(4)}$

https://doi.org/10.1021/acs.nanolett.4c05951
Nano Lett. 2025, 25, 4291−4297

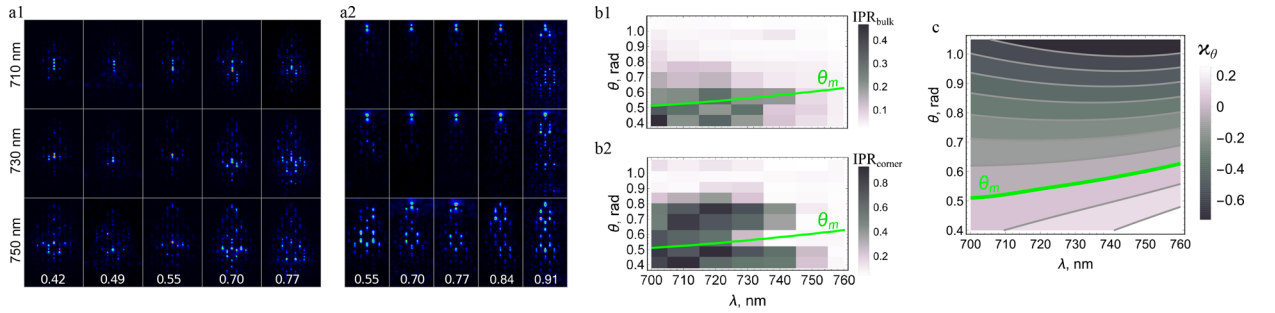

Figure 5. Wavelength dependence of caging and corner-localized dynamics. (a) Output intensity profiles for bulk (a1) and corner (a2) site laser excitations for a selected set of wavelengths and angles (indicated). (b) IPR for the bulk (b1) and corner (b2) site excitations obtained from the propagated intensity profiles, with the numerical invisibility angle dependence shown by a green curve. (c) Numerical nearest-neighbor $p-p$ coupling κ_θ as a function of the wavelength and the angle θ, showing a larger invisibility angle at larger wavelengths.

primitive generator class for C_2-symmetric systems.[57] Finite-lattice calculations utilizing the full Hamiltonian (eq 1) confirm the existence of the corner state in the entire interval of angles θ, with stronger localization arising close to the invisibility angle, Figure 4b.

In our experiments, we excite the corner p-waveguide using a spatial light modulator (SLM) image setup. We then image the field distribution at the output facet and extract the inverse participation ratio (IPR) quantifying the localization of the field. The results for the different lattices (i.e., different angles θ) are presented in Figure 4c. These results suggest that the IPR experiences a rapid decrease at angles $\theta > 0.8$, signaling less effective excitation of the corner mode. In this region of θ, the corner mode becomes less localized, developing a broader tail which degrades the efficiency of a single-site excitation.

WAVELENGTH DEPENDENCE OF THE INVISIBILITY ANGLE

Interestingly, invisibility angle physics and the designed quasi-flat band lattice can be readily reconfigured by changing the excitation wavelength. In our experiments, we use free-space single-site excitation from a supercontinuum laser source[48] in the wavelength range $\lambda \in \{700, 760\}$ nm for 7 representative wavelengths. The obtained results depicted in Figure 5a1,a2 suggest that the flat-band caging dynamics and the corner state localization are both preserved up to a wavelength $\lambda < 750$ nm. At larger wavelengths, the modes become more extended and the influence of long-range couplings deteriorates the overall caging effect.

The retrieved localization (IPR) of the output field for various θ and wavelengths is color-coded in Figure 5b1,b2 for both the bulk and corner excitations, indicating the presence of stronger caging in darker regions of the plot. We observe a gradual growth of the invisibility angle with the excitation wavelength, which aligns with numerical simulations in Figure 5c and opens a route toward photonic caging tunable by the excitation wavelength. A similar trend in the invisibility angle is observed when the distance d between the waveguides is decreased.[48]

In summary, we observed experimentally and confirmed numerically an invisibility angle phenomenon for p-mode photonic waveguides, evidencing a complete cancellation of coupling and an effective invisibility for a particular waveguide alignment. Importantly, for a given geometrical configuration, the near-invisibility-angle p-mode waveguide could be fine-tuned by changing the operating wavelength, providing a switchable coupler with all-optical control over the coupling efficiency.

The p-mode graphene-like lattice possesses a nearly all-band-flat phase with a highly localized and relatively long-lasting caging effect. To the best of our knowledge, our observation constitutes the first demonstration of such behavior in periodic and linear two-dimensional lattice systems serving as an alternative to the celebrated condensed-matter proposal of a dice lattice in the magnetic field,[40] which is challenging to implement in current photonic systems. As band dispersion could be tuned by the excitation wavelength, this allows one to switch from caging to dispersive dynamics. Therefore, our platform may find applications in optical and photonic on-chip technologies, such as diffractionless light guidance[58] and diffractionless image transmission.[59] Furthermore, an additional modulation of the waveguides along their axes could allow shifting of the entire field distribution in the transverse direction without the diffraction, similar to proposals in one-dimensional lattices.[6,60−62] From a fundamental perspective, the p-mode lattice near the invisibility angle demonstrates the significance of longer-range couplings and nonorthogonality corrections in the ABF regime.

The formation of a higher-order topological corner-localized state was clearly observed for the entire range of lattice geometries, providing an additional propagation channel, which is partially protected by the on-site p-mode symmetries. Both caging phenomenon and corner mode dynamics are most pronounced for shorter wavelengths, where the influence of long-range couplings and mode nonorthogonality is less important.

We anticipate that the similar invisibility angle phenomenon arises for higher-order orbital modes, transforming this idea into a broad physical concept. Such multipolar modes could be utilized to suppress not only nearest neighbor but also next-nearest neighbor couplings enabling the systematic construction of flat bands in electromagnetic, acoustic, and condensed matter systems and consolidating our observation as a beginning of orbital physics engineering.

ASSOCIATED CONTENT

Supporting Information

The Supporting Information is available free of charge at https://pubs.acs.org/doi/10.1021/acs.nanolett.4c05951.

Numerical calculation of the couplings from the eigenmodes of a dimer; evaluation of nonorthogonality corrections for waveguide lattices; construction of Bloch Hamiltonian and Wannier center calculation; computa-

https://doi.org/10.1021/acs.nanolett.4c05951
Nano Lett. 2025, 25, 4291−4297

tion of the inverse participation ratio; description of the femtosecond laser writing technique; further details on experiments (PDF)

AUTHOR INFORMATION

Corresponding Authors

Rodrigo A. Vicencio − *Departamento de Física and Millenium Institute for Research in Optics—MIRO, Facultad de Ciencias Físicas y Matemáticas, Universidad de Chile, 8370448 Santiago, Chile*; Email: rvicencio@uchile.cl

Maxim A. Gorlach − *School of Physics and Engineering, ITMO University, Saint Petersburg 197101, Russia*; orcid.org/0000-0002-7880-8953; Email: m.gorlach@metalab.ifmo.ru

Authors

Diego Román-Cortés − *Departamento de Física and Millenium Institute for Research in Optics—MIRO, Facultad de Ciencias Físicas y Matemáticas, Universidad de Chile, 8370448 Santiago, Chile*; orcid.org/0000-0001-8844-4236

Maxim Mazanov − *School of Physics and Engineering, ITMO University, Saint Petersburg 197101, Russia*

Complete contact information is available at: https://pubs.acs.org/10.1021/acs.nanolett.4c05951

Author Contributions

¶D.R.-C. and M.M. have equally contributed to this work.

Notes

The authors declare no competing financial interest.

ACKNOWLEDGMENTS

Theoretical models describing flat band formation were supported by the Russian Science Foundation (Grant 24-72-10069). Numerical studies of waveguide coupling were supported by Priority 2030 Federal Academic Leadership Program. M.M. and M.A.G. acknowledge partial support from the Foundation for the Advancement of Theoretical Physics and Mathematics "Basis". Experimental and other numerical studies were supported by Millennium Science Initiative Program ICN17_012 and FONDECYT Grant 1231313.

REFERENCES

(1) Szameit, A.; Nolte, S. Discrete optics in femtosecond-laser-written photonic structures. *Journal of Physics B: Atomic, Molecular and Optical Physics* **2010**, *43*, 163001.

(2) Rechtsman, M. C.; Zeuner, J. M.; Plotnik, Y.; Lumer, Y.; Podolsky, D.; Dreisow, F.; Nolte, S.; Segev, M.; Szameit, A. Photonic Floquet topological insulators. *Nature* **2013**, *496*, 196−200.

(3) Szameit, A.; Rechtsman, M. C. Discrete nonlinear topological photonics. *Nat. Phys.* **2024**, *20*, 905−912.

(4) Haus, H.; Huang, W.; Kawakami, S.; Whitaker, N. Coupled-mode theory of optical waveguides. *J. Lightwave Technol.* **1987**, *5*, 16−23.

(5) Keil, R.; Poli, C.; Heinrich, M.; Arkinstall, J.; Weihs, G.; Schomerus, H.; Szameit, A. Universal Sign Control of Coupling in Tight-Binding Lattices. *Phys. Rev. Lett.* **2016**, *116*, 213901.

(6) Cáceres-Aravena, G.; Guzmán-Silva, D.; Salinas, I.; Vicencio, R. A. Controlled Transport Based on Multiorbital Aharonov-Bohm Photonic Caging. *Phys. Rev. Lett.* **2022**, *128*, 256602.

(7) Mukherjee, S.; Di Liberto, M.; Öhberg, P.; Thomson, R. R.; Goldman, N. Experimental Observation of Aharonov-Bohm Cages in Photonic Lattices. *Phys. Rev. Lett.* **2018**, *121*, 075502.

(8) Eichelkraut, T.; Weimann, S.; Stützer, S.; Nolte, S.; Szameit, A. Radiation-loss management in modulated waveguides. *Opt. Lett.* **2014**, *39*, 6831.

(9) Weimann, S.; Kremer, M.; Plotnik, Y.; Lumer, Y.; Nolte, S.; Makris, K. G.; Segev, M.; Rechtsman, M.; Szameit, A. Topologically protected bound states in photonic parity−time-symmetric crystals. *Nat. Mater.* **2017**, *16*, 433−438.

(10) Vicencio, R.; Román-Cortés, D.; Rubio-Saldías, M.; Vildoso, P.; Foa Torres, L. Non-Reciprocal Coupling in Photonics. *arXiv* **2024**, 2407.18174. Accessed Jan 11, 2025.

(11) Longhi, S. Quantum-optical analogies using photonic structures. *Laser Photonics Rev.* **2009**, *3*, 243−261.

(12) Mazanov, M.; Román-Cortés, D.; Cáceres-Aravena, G.; Cid, C.; Gorlach, M. A.; Vicencio, R. A. Photonic Molecule Approach to Multiorbital Topology. *Nano Lett.* **2024**, *24*, 4595−4601.

(13) Ozawa, T.; Price, H. M.; Amo, A.; Goldman, N.; Hafezi, M.; Lu, L.; Rechtsman, M. C.; Schuster, D.; Simon, J.; Zilberberg, O.; Carusotto, I. Topological photonics. *Rev. Mod. Phys.* **2019**, *91*, 015006.

(14) Khanikaev, A. B.; Hossein Mousavi, S.; Tse, W.-K.; Kargarian, M.; MacDonald, A. H.; Shvets, G. Photonic topological insulators. *Nat. Mater.* **2013**, *12*, 233−239.

(15) Cáceres-Aravena, G.; Torres, L. E. F. F.; Vicencio, R. A. Topological and flat-band states induced by hybridized linear interactions in one-dimensional photonic lattices. *Phys. Rev. A* **2020**, *102*, 023505.

(16) Savelev, R. S.; Gorlach, M. A. Topological states in arrays of optical waveguides engineered via mode interference. *Phys. Rev. B* **2020**, *102*, 161112.

(17) Schulz, J.; Noh, J.; Benalcazar, W. A.; Bahl, G.; von Freymann, G. Photonic quadrupole topological insulator using orbital-induced synthetic flux. *Nat. Commun.* **2022**, *13*, 1−6.

(18) Mazanov, M.; Kupriianov, A. S.; Savelev, R. S.; He, Z.; Gorlach, M. A. Multipole higher-order topology in a multimode lattice. *Phys. Rev. B* **2024**, *109*, l201122.

(19) Danieli, C.; Andreanov, A.; Leykam, D.; Flach, S. Flat band fine-tuning and its photonic applications. *Nanophotonics* **2024**, *13*, 3925−3944.

(20) Danieli, C.; Andreanov, A.; Mithun, T.; Flach, S. Nonlinear caging in all-bands-flat lattices. *Phys. Rev. B* **2021**, *104*, 085131.

(21) Cáceres-Aravena, G.; Nedić, M.; Vildoso, P.; Gligorić, G.; Petrovic, J.; Maluckov, A.; Vicencio, R. A. Compact Topological Edge States in Flux-Dressed Graphenelike Photonic Lattices. *Phys. Rev. Lett.* **2024**, *133*, 116304.

(22) Cao, Y.; Fatemi, V.; Fang, S.; Watanabe, K.; Taniguchi, T.; Kaxiras, E.; Jarillo-Herrero, P. Unconventional superconductivity in magic-angle graphene superlattices. *Nature* **2018**, *556*, 43−50.

(23) Heikkilä, T. T.; Volovik, G. E. In *Basic Physics of Functionalized Graphite*; Esquinazi, P. D., Ed.; Springer International Publishing: Cham, Switzerland, 2016; pp 123−143.

(24) Pyykkönen, V. A. J.; Peotta, S.; Törmä, P. Suppression of Nonequilibrium Quasiparticle Transport in Flat-Band Superconductors. *Phys. Rev. Lett.* **2023**, *130*, 216003.

(25) Ciarrocchi, A.; Tagarelli, F.; Avsar, A.; Kis, A. Excitonic devices with van der Waals heterostructures: valleytronics meets twistronics. *Nat. Rev. Mater.* **2022**, *7*, 449−464.

(26) Hu, G.; Qiu, C.-W.; Alù, A. Twistronics for photons: opinion. *Optical Materials Express* **2021**, *11*, 1377.

(27) Zhou, X.; Lin, Z.-K.; Lu, W.; Lai, Y.; Hou, B.; Jiang, J.-H. Twisted Quadrupole Topological Photonic Crystals. *Laser Photonics Rev.* **2020**, *14*, 2000010.

(28) Flach, S.; Leykam, D.; Bodyfelt, J. D.; Matthies, P.; Desyatnikov, A. S. Detangling flat bands into Fano lattices. *EPL (Europhysics Letters)* **2014**, *105*, 30001.

(29) Maimaiti, W.; Andreanov, A.; Park, H. C.; Gendelman, O.; Flach, S. Compact localized states and flat-band generators in one dimension. *Phys. Rev. B* **2017**, *95*, 115135.

(30) Maimaiti, W.; Flach, S.; Andreanov, A. Universal $d = 1$ flat band generator from compact localized states. *Phys. Rev. B* **2019**, *99*, 125129.
(31) Maimaiti, W.; Andreanov, A.; Flach, S. Flat-band generator in two dimensions. *Phys. Rev. B* **2021**, *103*, 165116.
(32) Morales-Inostroza, L.; Vicencio, R. A. Simple method to construct flat-band lattices. *Phys. Rev. A* **2016**, *94*, 043831.
(33) Leykam, D.; Andreanov, A.; Flach, S. Artificial flat band systems: from lattice models to experiments. *Advances in Physics: X* **2018**, *3*, 1473052.
(34) Leykam, D.; Flach, S. Perspective: Photonic flatbands. *APL Photonics* **2018**, *3*, 070901.
(35) Vicencio Poblete, R. A. Photonic flat band dynamics. *Adv. Phys.: X* **2021**, *6*, 1878057.
(36) Zhu, W.; Zou, H.; Ge, Y.; Wang, Y.; Cheng, Z.; Wang, B.-b.; Yuan, S.-q.; Sun, H.-x.; Xue, H.; Zhang, B. Flatbands from Bound States in the Continuum for Orbital Angular Momentum Localization. *arXiv* **2024**, 2410.04040. Accessed Jan 11, 2025.
(37) Jörg, C.; Queraltó, G.; Kremer, M.; Pelegrí, G.; Schulz, J.; Szameit, A.; von Freymann, G.; Mompart, J.; Ahufinger, V. Artificial gauge field switching using orbital angular momentum modes in optical waveguides. *Light Sci. Appl.* **2020**, *9*, 150.
(38) Pelegrí, G.; Marques, A. M.; Dias, R. G.; Daley, A. J.; Mompart, J.; Ahufinger, V. Topological edge states and Aharanov-Bohm caging with ultracold atoms carrying orbital angular momentum. *Phys. Rev. A* **2019**, *99*, 023613.
(39) Mazanov, M.; Kupriianov, A.; He, Z.; Savelev, R.; Gorlach, M. *2023 Light Conference*; IEEE, 2023; pp 11−16.
(40) Vidal, J.; Mosseri, R.; Douçot, B. Aharonov-Bohm Cages in Two-Dimensional Structures. *Phys. Rev. Lett.* **1998**, *81*, 5888−5891.
(41) Longhi, S. Aharonov-Bohm photonic cages in waveguide and coupled resonator lattices by synthetic magnetic fields. *Opt. Lett.* **2014**, *39*, 5892−5895.
(42) Naud, C.; Faini, G.; Mailly, D. Aharonov-Bohm Cages in 2D Normal Metal Networks. *Phys. Rev. Lett.* **2001**, *86*, 5104−5107.
(43) Barsukova, M.; Grisé, F.; Zhang, Z.; Vaidya, S.; Guglielmon, J.; Weinstein, M. I.; He, L.; Zhen, B.; McEntaffer, R.; Rechtsman, M. C. Direct observation of Landau levels in silicon photonic crystals. *Nat. Photonics* **2024**, *18*, 580−585.
(44) Yang, J.; Li, Y.; Yang, Y.; Xie, X.; Zhang, Z.; Yuan, J.; Cai, H.; Wang, D.-W.; Gao, F. Realization of all-band-flat photonic lattices. *Nat. Commun.* **2024**, *15*, 1484.
(45) Hestand, N. J.; Spano, F. C. Expanded Theory of H- and J-Molecular Aggregates: The Effects of Vibronic Coupling and Intermolecular Charge Transfer. *Chem. Rev.* **2018**, *118*, 7069−7163. PMID: 29664617.
(46) Kazmaier, P. M.; Hoffmann, R. A Theoretical Study of Crystallochromy. Quantum Interference Effects in the Spectra of Perylene Pigments. *J. Am. Chem. Soc.* **1994**, *116*, 9684−9691.
(47) Yariv, A.; Yeh, P. *Optical Waves in Crystals: Propagation and Control of Laser Radiation*, Wiley Classics Library ed.; John Wiley and Sons: Hoboken, N.J, 2003.
(48) See Supporting Information for the numerical calculation of couplings from the eigenmodes of a dimer, evaluation of non-orthogonality corrections for waveguide lattices, construction of Bloch Hamiltonian and Wannier center calculation, computation of the inverse participation ratio, description of the femtosecond laser writing technique, and further details on experiments.
(49) Maczewsky, L. J.; Weimann, S.; Kremer, M.; Heinrich, M.; Szameit, A. *2019 Conference on Lasers and Electro-Optics (CLEO)*; IEEE, 2019; pp 05−10.
(50) Schulz, J.; Jörg, C.; von Freymann, G. Geometric control of next-nearest-neighbor coupling in evanescently coupled dielectric waveguides. *Opt. Express* **2022**, *30*, 9869−9877.
(51) Thouless, D. Electrons in disordered systems and the theory of localization. *Phys. Rep.* **1974**, *13*, 93−142.
(52) Leykam, D.; Bahat-Treidel, O.; Desyatnikov, A. S. Pseudospin and nonlinear conical diffraction in Lieb lattices. *Phys. Rev. A* **2012**, *86*, 031805.
(53) Vicencio, R. A.; Cantillano, C.; Morales-Inostroza, L.; Real, B.; Mejía-Cortés, C.; Weimann, S.; Szameit, A.; Molina, M. I. Observation of Localized States in Lieb Photonic Lattices. *Phys. Rev. Lett.* **2015**, *114*, 245503.
(54) Mukherjee, S.; Spracklen, A.; Choudhury, D.; Goldman, N.; Öhberg, P.; Andersson, E.; Thomson, R. R. Observation of a Localized Flat-Band State in a Photonic Lieb Lattice. *Phys. Rev. Lett.* **2015**, *114*, 245504.
(55) Mukherjee, S.; Thomson, R. R. Observation of robust flat-band localization in driven photonic rhombic lattices. *Opt. Lett.* **2017**, *42*, 2243−2246.
(56) Su, W. P.; Schrieffer, J. R.; Heeger, A. J. Solitons in Polyacetylene. *Phys. Rev. Lett.* **1979**, *42*, 1698−1701.
(57) Benalcazar, W. A.; Li, T.; Hughes, T. L. Quantization of fractional corner charge in C_n-symmetric higher-order topological crystalline insulators. *Phys. Rev. B* **2019**, *99*, 245151.
(58) Jang, B.; Gargiulo, J.; Ando, R. F.; Lauri, A.; Maier, S. A.; Schmidt, M. A. Light guidance in photonic band gap guiding dual-ring light cages implemented by direct laser writing. *Opt. Lett.* **2019**, *44*, 4016−4019.
(59) Yang, J.; Zhang, P.; Yoshihara, M.; Hu, Y.; Chen, Z. Image transmission using stable solitons of arbitrary shapes in photonic lattices. *Opt. Lett.* **2011**, *36*, 772−774.
(60) Brosco, V.; Pilozzi, L.; Fazio, R.; Conti, C. Non-Abelian Thouless pumping in a photonic lattice. *Phys. Rev. A* **2021**, *103*, 063518.
(61) Sun, Y.-K.; Zhang, X.-L.; Yu, F.; Tian, Z.-N.; Chen, Q.-D.; Sun, H.-B. Non-Abelian Thouless pumping in photonic waveguides. *Nat. Phys.* **2022**, *18*, 1080−1085.
(62) Röntgen, M.; Morfonios, C. V.; Brouzos, I.; Diakonos, F. K.; Schmelcher, P. Quantum Network Transfer and Storage with Compact Localized States Induced by Local Symmetries. *Phys. Rev. Lett.* **2019**, *123*, 080504.

https://doi.org/10.1021/acs.nanolett.4c05951
Nano Lett. 2025, 25, 4291−4297